

1 **Spectroscopic study of impurities and associated defects in nanodiamonds**  
2 **from Efremovka (CV3) and Orgueil (CI) meteorites**

3

4 A. A. Shiryaev<sup>1,\*</sup>, A. V. Fisenko<sup>2</sup>, I. I. Vlasov<sup>3</sup>, L. F. Semjonova<sup>2</sup>, P. Nagel<sup>4</sup>, S.  
5 Schuppler<sup>4</sup>

6

7 1) Institute of Physical Chemistry and Electrochemistry RAS, Leninsky pr.  
8 31, Moscow 119991, Russia

9 2) Vernadsky Institute of Geochemistry and Analytical Chemistry RAS,  
10 Kosygina Str. 19, Moscow, Russia

11 3) General Physics Institute RAS, Vavilov Str., 38, 119991 Moscow, Russia

12 4) Karlsruhe Institute of Technology, Institute für Festkörperphysik,  
13 Karlsruhe 76133, Germany

14

15 \* Corresponding author: shiryaev@phyche.ac.ru

16

17

18 **Abstract** – The results of spectroscopic and structural studies of phase composition and of  
19 defects in nanodiamonds from Efremovka (CV3) and Orgueil (CI) chondrites indicate that  
20 nitrogen atomic environment in meteoritic nanodiamonds (MND) is similar to that observed  
21 in synthetic counterparts produced by detonation and by the Chemical Vapour Deposition  
22 (CVD)-process. Most of the nitrogen in MND appears to be confined to lattice imperfections,  
23 such as crystallite/twin boundaries and other extended defects, while the concentration of  
24 nitrogen in the MND lattice is low. It is suggested that the N-rich sub-population of MND  
25 grains may have been formed with high growth rates in environments rich in accessible N  
26 (i.e., N in atomic form or as weakly bonded compounds). For the first time the silicon-  
27 vacancy complex (the “silicon” defect) is observed in MND by photoluminescence  
28 spectroscopy.

29

## 1. INTRODUCTION

30 Nanodiamonds in primitive carbonaceous chondrites contain high nitrogen contents  
31 (1–4 wt%) (Russell et al., 1996; Newton et al., 1995). The main peak of N release from  
32 samples of meteoritic nanodiamonds (MND) during step oxidation coincides with that of  
33 carbon (450–550 °C), thus strongly favoring the hypothesis that the N resides in diamond  
34 grains (Lewis et al., 1987; Newton et al., 1995; Russell et al., 1996; Verchovsky et al., 1998).  
35 Russell et al. (1996) reported a correlation between the nanodiamond content in meteorites  
36 and the N concentration in the MND. Low C/N ratio (25–100) in diamonds from the least  
37 metamorphosed chondrites (Acfer 094, ungrouped Orgueil, CI) suggests the existence of N-  
38 enriched (up to several wt% N) population of MND (Russell et al., 1996; Fisenko and  
39 Semjonova, 2006). It has been suggested (Fisenko et al., 1992) that thermal metamorphism of  
40 the meteorite body results in preferential destruction of the N-rich nanodiamonds and  
41 increase of C/N ratio in diamonds (e.g., up to  $242 \pm 32$  in Indarch (EH4), Russell et al., 1996).  
42 This scenario is supported by the higher oxidation rate of macrodiamonds with nitrogen  
43 concentrations exceeding a threshold value of  $\sim 1000$  ppm (Zhdankina et al., 1986).

44

45 It has been demonstrated experimentally that the efficiency of N incorporation into a  
46 diamond lattice during the Chemical Vapour Deposited (CVD-process) usually does not  
47 exceed  $10^{-3}$ , thus making impossible significant levels of diamond doped by nitrogen (Jin and  
48 Moustakas, 1994; Samlenski et al., 1995). The concentration of nitrogen in diamond grains in  
49 the CVD films rarely exceeds 200–300 ppm and is largely determined by the stability of  
50 nitrogenous compounds present in the growth chamber.

51 A much higher N content (up to 3 wt%) is found in Ultra Nano-Crystalline Diamond  
52 films (UNCD) (Zhang et al., 1999). These films are characterized by extremely small  
53 diamond grain sizes (5 to 50 nm) and grain boundaries of different configurations with widths

54 of several Ångstroms. However, in these films the N concentration in *diamond grains* is  
55 much lower and does not exceed 0.2 wt% (Birrell et al., 2003). The excess nitrogen is present  
56 as  $C_xN_y$  compounds (e.g., Zhang et al., 1999), probably at grain boundaries (Birrell et al.,  
57 2003; Zapol et al., 2001).

58 At the same time, detonation nanodiamonds (often called Ultra-Dispersed Diamonds –  
59 UDD) routinely produced by detonation of high-energy explosives in closed volumes (e.g.,  
60 Dolmatov et al., 2007) contain considerable amounts of nitrogen (up to 3%) as well as H and  
61 O and are, in this respect, broadly similar to meteoritic nanodiamond. It is believed that UDD  
62 are formed behind the shock wave front on a time scale of 0.1 to 0.5 microseconds from  
63 carbon liberated from organic compounds (Staver et al., 1984). The average size of diamond  
64 grains varies from 3 to 8 nm, though a tail up to ~12 nm is often observed (Anisichkin et al.,  
65 1988; Vlasov et al., 2010). Theoretical calculations suggest that incorporation of nitrogen into  
66 a nanodiamond grain with a high surface/bulk ratio is energetically unfavorable (Barnard and  
67 Sternberg, 2007). However, recent high resolution studies of UDD by Electron Energy Loss  
68 Spectroscopy (EELS) showed that N is indeed located within the diamond grains, but is  
69 usually associated with extended defects such as grain and crystallite boundaries (Kvit et al.,  
70 2003, Turner et al., 2009, Vlasov et al., 2010). The results of an X-ray Photoelectron  
71 Spectroscopy (XPS) study of UDD are also interpreted as an evidence for the presence of N  
72 in diamond grains (Dementjev et al., 2007).

73 The results summarized above lead to the following conclusions. If a diamond is  
74 synthesized in conditions where crystal growth depends on the kinetics of the absorption-  
75 desorption of carbon atoms and on the N partition ratio with a surrounding medium, i.e. not  
76 very far from equilibrium, the nitrogen content of the *diamond* phase (i.e. strictly  $sp^3$ -carbon  
77 with  $Fd3m$  space group) will be low ( $< \sim 0.3\text{--}0.4$  wt%). Such a situation is typical for  
78 terrestrial diamonds where the average N concentration is  $\sim 0.04$  wt%, and the maximum N

79 content is 0.3–0.35 wt% (Cartigny, 2005, Sellschop, 1992), as well for diamonds grown  
80 under High-Pressure-High-Temperature conditions (HPHT), which usually contain smaller  
81 amounts of N (~0.02 wt%). The highest reported values for HPHT diamonds are 0.33 wt%  
82 (Borzdov et al., 2002), i.e. similar to the maximum for natural macrodiamonds.

83 We note that the efficiency of nitrogen incorporation in the diamond lattice strongly  
84 depends on N speciation in the growth medium and on its partition ratio. Extensive studies of  
85 HPHT or CVD diamonds show that almost all nitrogen is incorporated as single  
86 substitutional atoms (Evans et al., 1992) and only a minor fraction ( $\sim 10^{-3}$ ) may be trapped as  
87 N-V-N complexes (Iakoubovskii et al., 2000a). Therefore, to achieve efficient incorporation,  
88 nitrogen in the growth medium should be present as single atoms or in weakly bound  
89 compounds.

90 When the diamond growth occurs in strongly non-equilibrium conditions, such as (but  
91 not limited to!) detonation synthesis, significant numbers of N atoms may be trapped inside  
92 the diamond grains, provided that N is abundant. Very fast linear growth rates in such cases  
93 makes the N incorporation rate largely insensitive to N speciation. Theoretical calculations of  
94 nitrogen behavior in detonation nanodiamonds (Barnard and Sternberg, 2007) and in UNCD  
95 (Zapol et al, 2001) show that it is much more favourable energetically to trap significant  
96 nitrogen concentrations at crystallite boundaries and extended defects than in the diamond  
97 lattice. This model appears to be supported also by experimental studies (Zhang et al., 1999,  
98 Vlasov et al., 2010). Metamorphic microdiamonds (sizes <300 microns) with high N content  
99 in the diamond lattice (up to 9600 ppm (Cartigny et al. 2004)) possibly deviate from this  
100 model but since their growth conditions and medium are not very well constrained, it is  
101 difficult to discuss them.

102 According to the proposed model, the MND grains enriched in N were probably  
103 formed in a non-equilibrium process in a medium with high nitrogen content. Verification of

104 this hypothesis requires investigation of impurity-related defects in MND with special  
105 emphasis on nitrogen-related defects.

106 Up to now, no reliable evidence of nitrogen-related defects in MND has been reported  
107 using optics-based spectroscopy (luminescence, absorption). In the case of macroscopic  
108 diamonds, infra-red (IR) spectroscopy permits quantitative investigation of nitrogen in the  
109 diamond lattice. Based only on their positions, some peaks in IR spectra of meteoritic  
110 nanodiamonds were ascribed to nitrogen point defects (Hill et al., 1997; Braatz et al., 2000).  
111 Such assignment is usually unacceptable in a single-crystal field, where the assignment is  
112 verified by matching the whole defect-induced one-phonon IR absorption spectrum rather  
113 than a single peak.

114 One of the main difficulties in many spectroscopic studies of nanodiamonds is the  
115 ubiquitous presence of non-diamond carbon and functionalisation of the nanodiamond  
116 surfaces by various C, O, H groups such as carboxyl, carbonyl etc. (Lewis et al., 1989;  
117 Bernatowicz et al., 1990; Jiang and Xu, 1995). Especially in studies where absorption spectra  
118 are acquired, the signals due to the non-diamond phases are often much stronger than those of  
119 nanodiamond or its bulk defects and impurities. Importantly, the IR spectra of dispersed  
120 nanodiamonds never show absorption by the diamond lattice itself in the two-phonon region.  
121 Possibly, the lattice absorption is not observed due to its relative weakness ( $13\text{ cm}^{-1}$ ) and the  
122 small amount of available meteoritic material (Hill et al., 1997; Braatz et al., 2000).  
123 Independently of the reason for the absence of the lattice absorption, the speculations about  
124 defect-related absorption in the one-phonon region are not justified. Moreover, as we will  
125 show below, nitrogen-related defects in MND are very different from those encountered in  
126 macrodiamonds and their IR absorption spectra are probably very different.

127 Here we report on the results of spectroscopic study of impurity-related defects in  
128 MND from Efremovka (CV3) and Orgueil (CI) chondrites using photoluminescence, Raman

129 and X-ray absorption spectroscopy. These results are compared with literature data for  
130 synthetic nanodiamonds produced by various methods. Implications for the MND formation  
131 process are discussed.

132

## 133 **2. SAMPLES AND METHODS**

134

135 The nanodiamond samples were extracted from the Efremovka, CV3 and the Orgueil, CI  
136 chondrites (DE1, DE2 and OD7, OD13, respectively) using a well-established process  
137 involving multistage chemical treatment by HF, HF+HCl, KOH, H<sub>2</sub>O<sub>2</sub>, K<sub>2</sub>Cr<sub>2</sub>O<sub>7</sub>, and HClO<sub>4</sub>  
138 at various temperatures and isolation of the colloidal nanodiamond at high pH values of the  
139 solution (Tang et al., 1988). The bulk samples DE1 and DE2 were obtained from aliquots of  
140 the same HF-HCl-resistant residue. However, for sample DE1 the aliquot was depleted by  
141 grains with density below 2 g/cm<sup>3</sup> as a result of heavy liquid sedimentation. For the bulk  
142 OD7 sample the acid-resistant residue was treated also by a mixture H<sub>3</sub>PO<sub>4</sub>+H<sub>2</sub>SO<sub>4</sub> (1:1) at  
143 220°C. Sample OD13 represents the fine-grained fraction remaining in the colloidal solution  
144 of the bulk OD7 sample aliquot after its ultracentrifugation (13500 g, 50 hours).

145 The difference between the grain sizes of the OD7 and OD13 samples appears to be  
146 correlated to differences in isotopic compositions of the carbon and xenon. According to the  
147 pyrolysis and combustion data of A. Verchovsky (Open University, Milton Keynes, UK) the  
148  $\delta^{13}\text{C}$  and  $^{136}\text{Xe}/^{132}\text{Xe}$  values for the OD7 are  $-34.5\pm 0.5\%$  and  $0.442\pm 0.004$ , respectively. For  
149 OD13, they are  $-28.1\pm 0.5\%$  and  $0.512\pm 0.004$ . All the samples possess a translucent pale  
150 yellow color, typical for meteoritic colloidal diamond. The masses of the samples studied  
151 were in the 1 to 3 mg range.

152 It is important to note that the samples studied were indeed nanodiamond material  
153 which was unambiguously proved by X-ray diffraction, Raman and X-ray absorption

154 spectroscopies (see below). In addition, the isotopic composition of nitrogen and noble gases  
155 is in the range reported previously for well-characterized samples of meteoritic nanodiamond  
156 (Russell et al., 1996, Huss and Lewis, 1994).

157 The average values of  $\delta^{15}\text{N}$  and C/N ratio for the DE1 and DE2 samples have been  
158 reported by Russell et al. (1996) are:  $213\pm 70$  (plateau) and  $-229.3\pm 8.6\text{‰}$  (bulk), respectively.  
159 For the OD7 and OD13 samples these values, as measured by A. Verchovsky, are  $75\pm 10$ , -  
160  $302\pm 5\text{‰}$  and  $58\pm 5$ ,  $-300\pm 5\text{‰}$ , correspondingly. The marked differences in the nitrogen  
161 concentrations and isotopic compositions between the Efremovka and Orgueil nanodiamonds  
162 are mostly due to different degrees of thermal metamorphism of their parent bodies (Russell  
163 et al., 1996).

164 A UDD sample treated by  $\text{HClO}_4$  (4h at  $220\text{ }^\circ\text{C}$ ) was used for comparative purposes  
165 in our spectroscopic study. The nitrogen environment in a similar sample was studied by  
166 Vlasov et al. (2010) by Electron Electron Loss Spectroscopy (EELS).

167 The Efremovka MND samples were investigated using X-ray diffraction (XRD),  
168 Small-Angle X-ray scattering (SAXS), photoluminescence (PL) spectroscopy at room and at  
169 liquid He (LHe) temperatures and by Raman spectroscopy using visible (514 nm) and UV  
170 (244 nm) lasers at room temperature. The Orgueil samples were studied by luminescence,  
171 SAXS and imaging Near Edge X-ray Absorption Spectroscopy (NEXAFS).

172 To exclude sample heating during the Raman and PL measurements, the samples  
173 were embedded into pure copper, thus dramatically minimizing artifacts due to thermal  
174 effects. Our extensive experiments on nanodiamonds of various origins have shown the  
175 reliability of such sample preparation. The Raman spectra of the Efremovka nanodiamonds  
176 were obtained using a UV laser (244 nm) at low laser power (1 to 2.5 mW). The majority of  
177 the PL measurements were performed using a LABRAM HR spectrometer with an Ar<sup>+</sup> laser  
178 (488 nm). The laser power was limited to 1 mW and the beam was focused to 2 to 5 microns



179 on the surface of the MND samples. The accuracy of the determination of the positions of the  
180 peaks in the PL spectra was  $\pm 0.1$  nm.

181 The nitrogen speciation in the MND from Orgueil and in the UDD was assessed by  
182 imaging Near Edge X-ray Absorption Fine Structure spectroscopy (NEXAFS). The  
183 measurements were performed at the WERA beamline at the ANKA synchrotron source,  
184 Karlsruhe. The samples of meteoritic and detonation nanodiamonds were prepared by drying  
185 drops of the colloidal solution of the MND and the water suspension of the UDD on a silicon  
186 or copper substrate. The C and N concentrations of the substrates were inferred from inert gas  
187 fusion and were far lower than the detection limit of the equipment employed. The samples  
188 were illuminated with monochromatic X-rays at an incident angle of  $25^\circ$  to their surface.  
189 Carbon and nitrogen absorption K-edges were analyzed. For the C K-edge the energy scans  
190 were performed between 280 eV and 315 eV, and for the N K-edge - between 395 eV and  
191 430 eV. Up to 15 consecutive scans were performed at the nitrogen edge to improve the  
192 signal to noise ratio. The energy resolution at the C K-edge was 0.1 eV; at the N K-edge -  
193 0.22 eV. The lateral distribution of the emitted electron intensity was mapped by means of a  
194 photoemission electron microscope (PEEM). The FOCUS IS-PEEM instrument used  
195 achieves a lateral resolution of  $\sim 100$  nm at the energies employed.

196 The NEXAFS information on the chemical bonding and local electronic structure  
197 around the absorbing atom is obtained from the spectral X-ray scan. For each step of the X-  
198 ray energy, a PEEM image was recorded representing the laterally resolved electron emission  
199  $I(x, y)$  for a well defined excitation energy  $E$ . In this way, a four-dimensional data stack  $\{I(x,$   
200  $y), E\}$  was produced, from which NEXAFS spectra from arbitrary sample areas were  
201 extracted by plotting the integrated image intensity  $I$  of this specific area versus the photon  
202 energy  $E$  (Berg et al., 2006). Using the imaging mode the areas with small agglomerates of  
203 nanodiamonds where no charging was present were selected and analysed. Standard

204 corrections for dark and flat field were applied. The contribution from amorphous carbon on  
205 the X-ray optics was corrected by subtracting the spectra recorded at diamond-free parts of  
206 the silicon substrate.

207 Modeling of the NEXAFS spectra for several possible configurations of nitrogen in  
208 cubic and hexagonal diamond lattices was performed using feff8.2 software (Ankudinov et  
209 al., 1998). An atomic cluster with radius 6 Å around the central nitrogen atom was employed.  
210 The calculations were performed both for the unrelaxed lattice as well as for various degrees  
211 of lattice relaxation accounted for by preselected elongation of one or more C-N bonds. In  
212 addition, several calculations were performed for clusters containing a vacancy in the vicinity  
213 of the nitrogen impurity.

214

## 215 **3. RESULTS**

### 216 **3.1. X-ray diffraction**

217

218 Diamond reflections in the XRD patterns for MND are broad, which is due to small grain size  
219 and strain/defects (Fig. 1). The average size of the diamond crystallites (in the 111 direction)  
220 estimated from the width of the diffraction peaks is approximately 3 nm which is similar to  
221 the value obtained using transmission electron microscopy (2.6–2.8 nm, Lewis et al., 1989;  
222 Daulton et al., 1996). Similar values were also obtained by SAXS technique. In addition to  
223 obvious diamond reflections, a very weak peak corresponding to main graphite interlayer  
224 spacing is observed at 3.34 Å. This value is just slightly smaller than that for turbostratic  
225 graphite. From the relative intensity of the diamond 111 and graphite 002 peaks and  
226 corresponding values of efficiency of the reflections, the amount of graphite is estimated to  
227 be ~3–5 wt%. The presence of a broad halo at small diffraction angles (corresponds to high  
228 interplanar spacings) indicates that even the severe chemical treatment does not lead to

229 complete elimination of amorphous carbon. However, it is impossible to rigorously estimate  
230 the relative fraction of the amorphous phase.

231

## 232 **3.2. Spectroscopy**

### 233 *3.2.1. Raman spectroscopy*

234

235 Detection of the diamond Raman line in substances with a significant fraction of  $sp^2$ -bonded  
236 carbons is often challenging, since Raman scattering excited by visible radiation is more  
237 sensitive to  $\pi$ -bonding, which exists in carbon structures formed by  $sp^2$ -hybridised orbitals  
238 (C=C double bonds), whereas Raman scattering excited by UV radiation is more sensitive to  
239  $\sigma$ -bonding. The  $\sigma$ -bonds are present in all carbon materials, but they dominate in carbons  
240 with  $sp^3$ -hybridization (C-C single bonds). The photon energy of UV radiation with a  
241 wavelength of 244 nm is equal to 5.08 eV, which is close to the energy band gap between  
242 electronic states of  $\sigma$ -bonds (5.47 eV) in diamond. Thus employment of the 244 nm laser  
243 creates near-resonance conditions enhancing the Raman cross-section of diamond carbon  
244 (Ferrari and Robertson, 2004; Mikhaylyk et al., 2005). In addition, the characteristic  
245 luminescence of nanodiamonds is very weak at UV excitation.

246 The UV Raman spectra of the DE1 and DE2 samples are shown in Figure 2. A broad,  
247 asymmetric, downshifted diamond peak is clearly observed along with broad bands due to  
248 graphite-like carbon and C=O bonds. The presence of the C=O bonds is due to oxygen,  
249 chemisorbed on the surfaces of nanodiamond grains (Lewis et al., 1989). The diamond peak  
250 is observed at  $1327\text{ cm}^{-1}$  in the spectrum of sample DE1; the spectrum of sample DE2 is  
251 noisier, but the diamond peak is located at approximately the same wavenumber:  $1326\text{ cm}^{-1}$ .  
252 Spectra like those for DE1 and DE2 samples are typical for UDD (Vul', 2006).

253           The first order Raman spectrum of diamond consists of a single line at  $1332\text{ cm}^{-1}$ . At  
254   least two different phenomena which may act simultaneously could be responsible for the  
255   downshift of the Raman peak for the MND: (1) phonon confinement due to a decrease of  
256   diamond crystallites down to approx. 3 nm (Lipp et al., 1997), and (2) the presence of  
257   hexagonal diamond polytypes (hex-Dia). The average size of the grains in MND does not  
258   exceed 3 nm (Lewis et al., 1989, Daulton et al., 1996; our X-ray and SAXS measurements)  
259   and it is thus not surprising that size effects become pronounced in their Raman spectra.  
260   Though according to TEM, the fraction of purely hex-Dia particles is not very high, MND  
261   grains often contain stacking faults and other similar imperfections (Daulton et al., 1996).  
262   From a crystallographic point of view, many types of stacking faults in the cubic diamond  
263   lattice may be regarded as hexagonal polytypes. The Raman peaks of 2H and 6H diamond  
264   polytypes are located between  $1319$  and  $1327\text{ cm}^{-1}$  (Knight and White, 1989) Therefore, at  
265   least partially, the observed downshift may be due to such extended defects.

266

### 267   3.2.2. Photoluminescence

268

269           The photoluminescence spectra of the samples studied at room- and liquid helium  
270   temperatures are broadly similar (Fig. 3a, see also Shiryaev et al., 2009). Such similarity  
271   indicates inhomogeneous, i.e. strain-related (e.g., Davies, 1970), line broadening as is  
272   expected for nanoparticles. The spectra are dominated by a broad band with a maximum  
273   around 560 nm (red emission) with shoulders around 530 and 610 nm. Such spectra are  
274   typical for UDD. The broad band probably represents overlapping signals from non-diamond  
275   carbon and from defects on the surfaces of diamond grains (Iakoubovskii et al., 2000b; Smith  
276   et al., 2008). It is not yet known if nanodiamonds synthesized by homogeneous nucleation  
277   and growth in the vapor phase (i.e., CVD-like processes) exhibit similar spectral features.

278 The PL spectra were recorded over a broad wavelength range, which allowed  
279 observation of a remarkable feature at 737 nm (1.681 eV) with a weak shoulder around 757  
280 nm (Fig. 3b). Several luminescent centers in diamond have peaks in this wavelength range:  
281 the “silicon” center (see below), the neutral vacancy (the GR1 center), and a zero-phonon line  
282 from a radiation-related defect. However, the GR1 defect peaks at 741 nm, which is clearly  
283 different from the observed peak at 737 nm (the uncertainty of our measurements is  $\pm 0.1$   
284 nm). The radiation-related defect at 736 nm accompanies the GR1 defect, being much  
285 weaker. Therefore, the absence of the GR1 shows that the observed peak at 737 nm cannot be  
286 due to the radiation-related defect.

287 Presence of the main line (737 nm) and a prominent secondary line (757 nm) is an  
288 unambiguous manifestation of the well-known “silicon” defect, most probably consisting of a  
289 silicon ion in the divacancy (commonly called a silicon-vacancy complex or Si-V) (for a  
290 review see Zaitsev, 2001). The observed band is broad and the fine structure typical for this  
291 defect is not resolved due to size/strain effects and related inhomogeneous broadening. For  
292 comparison, a spectrum of a Si-V defect in nanocrystalline CVD film (Vlasov et al., 2009) is  
293 shown in Figure 3b. However, the observed band is still sufficiently narrow to be reliably  
294 ascribed to a defect in a crystalline lattice. Bands due to defects in (semi)amorphous local  
295 environment are invariably much broader. This defect is observed in Si implanted diamonds  
296 after annealing (Zaitsev et al., 1981), in CVD and UNCD films grown on Si substrate  
297 (Vavilov et al., 1980, Vlasov et al., 2009, Basov et al., 2009), and in synthetic (Clark et al.,  
298 1995) and natural macrodiamonds (Iakoubovskii et al., 2001). However, it is not observed in  
299 UDD, probably, due to the general absence of Si compounds in explosion chambers.

300

301 The relative intensity of the Si defect in spectra of the Efremovka nanodiamond is  
302 higher than in the Orgueil nanodiamonds (Fig. 3b). This may reflect different concentration

303 of the Si impurity in these samples. A comparison of the relative intensities of the Si defects  
304 in Orgueil nanodiamond samples with slightly different median sizes (Fig. 3b) shows that in  
305 the sample made of slightly finer grains (OD13 vs OD7), the Si defect is less pronounced.

306 Unfortunately, the concentration of silicon in the MND can not be determined from  
307 the luminescence measurements. Initial attempts to obtain qualitative information from  
308 absorption spectroscopy were unsuccessful due to the very small amount of material  
309 available. The study of the MND dispersed on a substrate show that the Si-V defects are  
310 present in many grains including the smallest ones (1 to 2 nm in size). A very rough estimate  
311 of the possible concentration of silicon in MND suggests values around tens of ppm.

312 To the best of our knowledge, this is the first observation of the silicon defect not only  
313 in meteoritic, but in any type of dispersed nanodiamond.

314 Note that a defect present in all types of irradiated diamonds, the GR1, is absent in  
315 spectra of the samples studied here (see above). As follows from the name of this defect  
316 (*General Radiation*), this defect appears after any type of irradiation. Its absence might imply  
317 that the irradiation of the MND was very moderate. However, this statement should be treated  
318 with caution, since the efficiency of GR1 generation strongly depends on the concentration  
319 and type of other defects present in the diamond and has been insufficiently studied for  
320 nanoparticles. Alternatively, the radiation defects may have been annealed before the  
321 formation of the parent bodies and prior to capture of the P3 noble gas component by the  
322 MND.

323 Spectra of MND samples kept in air for several years prior to the room temperature  
324 PL study sometimes showed existence of a broad PL band at 500 nm, rapidly vanishing even  
325 under low laser power. This feature is most likely due to some carbonaceous contamination,  
326 which builds up during storage. This contamination could also be responsible for the increase

327 in  $\delta^{13}\text{C}$  for carbon released from MND at low oxidation temperatures (Russell et al., 1996).  
328 The carbonaceous contamination is also observed in C NEXAFS spectra (see below).

329

### 330 **3.3. Imaging NEXAFS and Photoelectron Emission Microscopy (PEEM)**

331

332 Figure 4 shows a PEEM image of the MND from Orgueil at an incident energy of  
333 293 eV, i.e. above the C absorption edge. The nanodiamonds are clearly visible as white  
334 (emitting) regions. Several nanodiamond-rich regions of the image stacks were selected and  
335 their C and N NEXAFS spectra were analyzed. Nanodiamond-free areas were used to correct  
336 for C contamination of the beamline optics.

337 Figure 5a shows the carbon edge for the UDD and for the MND from Orgueil (sample  
338 OD7). The spectra are typical for macro- and nanodiamonds (Morar et al., 1985, Birrell et al.,  
339 2003, Berg et al., 2008). They show the typical features of diamond: an absorption edge  
340 representing the conduction band edge, a C 1s core exciton, a series of structures resulting  
341 from a band of  $\sigma^*$  states, and the second absolute band gap. The relative intensities of the  
342 features around the absorption edge could be slightly different from an ideal diamond due to  
343 difficulties in subtraction of the background in this region. Note the presence of a small peak  
344 at 285 eV indicating a small amount of  $sp^2$ -carbon (graphitic and/or aromatic), also typical  
345 for nanodiamonds. Similar to the Murchison nanodiamond (Berg et al., 2008), the sample  
346 from Orgueil shows a weak feature at 287 eV, which can be ascribed to semi-amorphous  
347 carbon on surfaces of nanodiamond grains, as also revealed by Raman spectroscopy.  
348 However, this feature is absent in the spectra of the UDD (Fig. 5a). The reason for such a  
349 discrepancy is not yet clear, but it may reflect differences in surface chemistry of UDD and  
350 MND.

351 The nitrogen absorption spectra (Fig. 5b) are relatively noisy. This clearly results  
352 from low concentrations of this element. In contrast to the spectrum of the UDD, a weak peak  
353 at 400 eV for the MND is obvious. This feature is most likely due to weakly  $\pi$ -bound  
354 nitrogen in a carbonaceous environment (Jimenez et al., 2001) probably corresponding to the  
355 (semi)amorphous outer shell which is also manifested in C NEXAFS and Raman spectra. The  
356 surface-bound nitrogen may have been chemisorbed during MND residence in space or  
357 during the separation procedure (Fisenko and Semjonova, 2006). The main absorption edge is  
358 observed at about 405 eV in the spectra of both the MND and the UDD. This position is  
359 indicative of N in  $sp^3$ -bonding configurations (see below). It should be noted that the N  
360 NEXAFS spectra of UNCD (Birrell et al., 2003) are similar to those observed in this study  
361 with the exception of the peak at 400 eV.

362

363

#### 4. DISCUSSION

364

365 Optics-related methods such as IR-Vis-UV absorption and photoluminescence (PL) as well as  
366 Electron Paramagnetic Resonance (EPR) are extremely sensitive to nitrogen defects in the  
367 diamond lattice. The N concentration in diamond determined by these methods correlates  
368 quantitatively with data obtained by nuclear probes and inert gas fusion (Davies, 1999,  
369 Sellschop, 1992). However, nitrogen in nanodiamond produced by detonation or by CVD is  
370 difficult to observe by the spectroscopic techniques mentioned above, and only recently  
371 reliable detection of N-V defects have been reported for nanodiamond particles of 5–10 nm in  
372 size (Bradac et al., 2010; Smith et al., 2008; Vlasov et al., 2010). The published data on  
373 nanodiamond spectroscopy set an upper limit to nitrogen-related defects in diamond lattice of  
374 several hundred ppm at most (Iakoubovskii et al., 2000b; Orlinskii et al., 2011). Comparison  
375 of the concentration of paramagnetic nitrogen in nanodiamonds measured by EPR with mass-



376 spectrometric determinations shows that the paramagnetic N atoms are always just a small  
377 fraction of the total N content of the samples (e.g., Orlinskii et al., 2011). The absence of  
378 clearly identified N-related signals in EPR spectra of MND implies that nitrogen in MND is  
379 predominantly non-paramagnetic (Braatz et al., 2000). In the current work, spectroscopic  
380 manifestations of the nitrogen-related defects in MND are also not observed (NEXAFS  
381 results are *not* considered yet).

382         Reconciliation of weakness of the spectroscopic manifestations of abundant structural  
383 N with the mass-spectrometry results showing N content of meteoritic and detonation  
384 nanodiamond as high as 1–2 wt% (Russell et al., 1996; Dolmatov, 2007) is not trivial. Note  
385 that the PL manifestations of the Si-V and the EPR spectrum of the proton-vacancy defects  
386 (the H1-defect, Braatz et al., 2000) in MND are fairly similar to manifestations of these  
387 defects in macrodiamonds if the strain-related broadening is taken into account. At the same  
388 time, the concentrations of the nitrogen-related defects observed are low. Several physical  
389 mechanisms could be responsible for considerable differences between the detection of the  
390 defects in nano- vs. bulk diamond by spectroscopic techniques.

391         1) The presence of 1–2 wt% of N in the diamond lattice inevitably produces  
392 considerable strains due to differences in C and N ionic radii. Configuration of the  
393 energy levels in a highly-strained nanodiamond grain as well as small distance  
394 between the defect and grain surface may allow efficient non-radiative de-  
395 excitation channels. As a result, some defects may possess very weak, if any, PL  
396 responses. In contrast to the NV, the “silicon” defect has very weak electron-  
397 phonon interaction, and the changes in the diamond density-of-states due to  
398 decreasing size should have smaller effect on spectral manifestations of the Si-V  
399 defect.

400 2) The structure of the N-related defects in a nanodiamond differs considerably from  
401 that in the bulk diamond.

402

403 The explanations provided are not mutually contradictory. However, the results of our  
404 NEXAFS study and previously published data (Birrell et al., 2003; Vlasov et al., 2010)  
405 suggests that differences in atomic structure of the N environments are very important.

406 Using the feff8.2 code (Ankudinov et al., 1998) we have performed theoretical  
407 modeling of N NEXAFS spectra in cubic and hexagonal diamond polytypes. Figure 5c shows  
408 modeled spectra for nitrogen configurations usually encountered in macrodiamonds:  
409 substitutional single and paired nitrogen atoms with several values of lattice relaxation, as  
410 well for some other configurations of several N atoms and vacancies. The modeled spectra  
411 differ from the experimental spectra. The spectra of nitrogen atoms surrounded by various  
412 arrangements of vacancies are characterized by fewer broad spectral features, making them  
413 qualitatively more similar to the observations. Results of our modelling are qualitatively  
414 similar to earlier calculations of EELS spectra of N in diamonds (Brydson et al., 1998).

415 The XPS spectra for N in UNCD and UDD suggest the presence of two or, perhaps,  
416 three types of N environment (Zhang et al., 1999; Dementjev et al., 2007). Although there is  
417 no unique interpretation of the N XPS and NEXAFS spectra in the C-N systems is not yet  
418 possible, the features observed may originate from nitrogen occupying two and three-  
419 coordinated structures with at least one of the nearest neighbours being also a two- or three-  
420 coordinated carbon (Titantah and Lamoen, 2007). This assignment is consistent with a  
421 suggestion that N is largely confined to grain- and intercrystallite boundaries and other  
422 extended defects in UNCD (Zapol et al., 2001; Birrell et al., 2001) and UDD (Vlasov et al.,  
423 2010).

424 Our N NEXAFS spectra of the MND can be represented as a superposition of a  
425 “sharp” feature at 400 eV and a broad absorption starting at 405 eV. The 400 eV peak is  
426 probably due to  $\pi$ -bonded, presumably chemisorbed N (see above). The broad absorption  
427 shows close resemblance to NEXAFS spectra of detonation nanodiamonds (Fig. 5) and  
428 UNCD (Birrell et al., 2003) and to N EELS spectra of UDD (Pichot et al., 2010). This  
429 similarity suggests that the average local environment of the main fraction of nitrogen  
430 impurity in MND, UDD and UNCD is similar. Following the XPS results (Zhang et al., 1999;  
431 Dementjev et al., 2007; Titantah and Lamoen, 2007), we suggest that N in these  
432 nanodiamonds is most likely distributed among several main atomic configurations, thus  
433 blurring the absorption spectra. However, the set of these configurations is not completely  
434 random and/or sample-dependent, which is indicated by the consistent shape of the  
435 absorption spectra. Therefore, the atomic-level N environment in MND is markedly different  
436 from the bulk diamond lattice and, therefore, its manifestations in IR absorption and  
437 luminescence must be different. This may explain the failure of reliable observation of N-  
438 related defects in MND (Braatz et al., 2000, Hill et al., 1997) by IR spectroscopy. Possibly,  
439 nitrogen in MND is largely segregated to extended defects such as crystallite and twin  
440 boundaries. According to a TEM study by Daulton et al. (1996), the concentration of twins in  
441 MND is not very high. However, this does not contradict the hypothesis that nitrogen in  
442 MND is mostly concentrated at extended imperfections, since the relative fraction of N-rich  
443 nanodiamond grains is unknown.

444

445 As discussed in the introduction, incorporation of high amounts of nitrogen (>1 wt%)  
446 into the diamond lattice is very difficult. N-rich nanocrystalline diamond films containing  
447 ~0.2 wt% of N are grown from a medium with high N (>10%) content. Linear growth rates of  
448 diamond crystallites in these films are usually low: <0.1  $\mu\text{m/h}$  (May and Mankelevich, 2007).

449 Presumably, such slow growth leads to formation of N-poor nanograins joined by N-rich  
450 grain boundaries. In contrast, the linear growth rate of N-rich UDD is very high and may  
451 reach  $10^5$  to  $10^6$   $\mu\text{m}/\text{h}$ . Presumably, the nitrogen atoms are simply buried by the carbon  
452 atoms. Preferential localization of N at the grain boundaries and between crystallites results  
453 from diffusion processes while the grain is still at high temperatures and from formation of  
454 N-poor “perfect” grains.

455 Application of this model of the formation of N-rich nanodiamonds to MND implies  
456 that these grains grew very fast in strongly non-equilibrium conditions and that their growth  
457 medium was rich in nitrogen in a form readily available for incorporation into the diamond  
458 structure.

459 Several modes of formation of MND with high amounts of nitrogen may be proposed.

460 1) Shock-induced transformation of the C-N-rich organics, for example, after  
461 supernovae explosion (Saslaw and Gaustad, 1969; Blake et al., 1988; Fisenko et  
462 al., 2001). Problems with this scenario are that several conditions should be  
463 achieved in the region of MND formation: a high density of starting matter and a  
464 high rate of temperature decrease. However, a density and temperature increase  
465 during the passage of a shock wave through a C-N rich gaseous medium may serve  
466 as an efficient trigger for fast disequilibrium growth of nanodiamonds, by, for  
467 example, a CVD-like process (see below). A somewhat similar process was  
468 employed in laser- or discharge-induced diamond growth (e.g., Buerki and  
469 Leutwyler, 1991).

470 2) Formation of nanodiamond in UV-irradiated ices and/or organics has been  
471 proposed by Nuth and Allen (1992). However, the growth rates currently obtained  
472 in experiments are low (Kouchi et al., 2005). The possibility of fast diamond  
473 growth by this mechanism, e.g., in a very intense flash of high energy photons, has

474 still to be checked experimentally. In any case, this mechanism does not seem very  
475 efficient since it requires simultaneous destruction of several chemical bonds in a  
476 solid substance and subsequent rearrangement into the diamond structure. The  
477 probability of this process increases with fluence, but, at high UV fluences the  
478 stability of nanodiamonds against graphitization decreases (Butenko et al., 2008).

479 3) The CVD-like process is a very attractive mechanism (Lewis et al., 1989; Daulton  
480 et al., 1996). However, to achieve a high N content in the diamond grains, it should  
481 occur in environments rich in accessible N (in atomic form or as weakly bonded  
482 compounds) and proceed with high growth rates. The possibility of nanodiamond  
483 growth by CVD-like processes with high linear growth rates (up to thousands  
484  $\mu\text{m/h}$ ) has been demonstrated (Buerki and Leutwyler, 1991; Frenklach et al., 1991;  
485 Palnichenko et al., 1999).

486 In our view, the fast CVD-like mechanism is the most plausible. The CVD-like  
487 mechanism of formation of interstellar nanodiamonds is supported by microscopic  
488 observations of Daulton et al. (1996).

489 The N-rich grains of MND may represent just one of the possible sub-populations of  
490 MND. The presence of several populations of nanodiamond grains with somewhat different  
491 properties can be inferred from variations of the C, N and noble gases isotopic compositions  
492 observed during stepped pyrolysis and oxidation of nanodiamonds from different petrological  
493 and chemical classes of meteorites (Huss and Lewis, 1994; Russell et al., 1996; Verchovsky  
494 et al., 1998).

495

496

## 5. CONCLUSIONS

497

498 Phase compositions and defects in nanodiamonds separated from Efremovka, CV3  
499 and Orgueil, CI chondrites were studied using Raman and photoluminescence spectroscopies  
500 at different excitation wavelengths, X-ray scattering and diffraction and X-ray absorption  
501 spectroscopy.

502 We show that the phase compositions of the meteoritic and the synthetic (detonation)  
503 nanodiamonds are similar, suggesting that both types of nanodiamonds presumably consist of  
504 a diamond core surrounded by (semi)amorphous and graphite-like carbon.

505 The nitrogen atomic environment appears to be broadly similar for meteoritic and  
506 detonation nanodiamonds as well as for Ultra-Nano-Crystalline CVD films. Most of the  
507 nitrogen in MND appears to be confined to lattice imperfections, such as crystallite/twin  
508 boundaries and other extended defects; the concentration of nitrogen in the MND lattice is  
509 low. This leaves little chance for success in the search for spectral manifestations of common  
510 N-related defects in meteoritic nanodiamonds.

511 The high nitrogen content in at least some MND grains suggests that their growth rate  
512 was high. One of the plausible formation mechanisms of MND is the CVD-like process in  
513 regions rich in accessible N (in atomic form or as weakly bonded compounds), possibly  
514 triggered by a shock wave. Other processes such as nanodiamond formation in irradiated  
515 organics can not be excluded. The subpopulation of N-rich nanodiamond grains could have  
516 formed both prior to and/or during Solar System formation. It seems unlikely that this  
517 subpopulation is a carrier of isotopically anomalous HL noble gases, which are presolar. This  
518 follows from negative correlation between contents of the nitrogen and the HL component of  
519 noble gases in nanodiamonds from meteorites subjected to different degrees of thermal  
520 metamorphism.

521 For the first time the silicon-vacancy complex (the “silicon” defect) has been  
522 observed in meteoritic nanodiamond by photoluminescence spectroscopy. Moreover, this is

523 the first observation of this defect in dispersed nanodiamonds of any origin. Study of Si  
524 isotopic composition in nanodiamonds may help to understand their origin. To avoid  
525 contributions from the SiC grains, the investigation of Si isotopes should be performed on  
526 nanodiamond grains isolated from metamorphosed meteorites such as, e.g., Allende, CV3 and  
527 Efremovka, CV3, or a chemical treatment destroying SiC should be employed.

528

529 *Acknowledgements:* Discussions with Drs K. Iakoubovskii and V. Krivobok on interpretation  
530 of luminescence results are highly appreciated. We are grateful to Dr. A. Verchovsky for  
531 provision of the bulk sample of the Orgueil meteorite and of the results of isotopic  
532 measurements of Orgueil nanodiamonds. Comments of Dr. T. Daulton on the early version of  
533 the manuscript as well as comments of anonymous reviewers are highly appreciated. We  
534 highly appreciate help of Dr. A.N. Krot and Dr. T. Lafford in improving of English. This  
535 work was supported by RFBR grant 08-05-00745a and Program RAS #21. ANKA  
536 (Angstroemquelle Karlsruhe) synchrotron radiation facility is acknowledged for the provision  
537 of beamtime (project MR-97).

538  
539  
540  
541  
542  
543  
544  
545  
546  
547  
548  
549  
550  
551  
552  
553  
554  
555  
556  
557  
558  
559  
560  
561

## References

- Anisichkin V. F., Mal'kov I. Yu., Titov V. M. (1988) Diamond synthesis at dynamic loading of organic compounds. *Dokl. Akad. Nauk SSSR* **303**, 625-627.
- Ankudinov A. L., Ravel B., Rehr J.J., and Conradson S.D. (1998) Real Space Multiple Scattering Calculation of XANES, *Phys. Rev.* **B 58**, 7565.
- Barnard A. S. and Sternberg M. (2007) Can we predict the location of impurities in diamond nanoparticles? *Diam. Relat. Mater.* **16**, 2078-2082.
- Basov A. A., Rahn M., Pars M., Vlasov I. I., Sildos I., Bolshakov A. P., Golubev V. G., and Ralchenko V. G. (2009) Spatial localization of Si-vacancy photoluminescent centers in a thin CVD nanodiamond film. *Phys. Status Solidi* **A206**, 2009-2011.
- Berg T., Maul J., Erdmann N., Bernhard P., Schuppler S., Nagel P., Sudek C., Ott U., and Schönhense G. (2006) Coupling of imaging NEXAFS with secondary ion mass spectrometry for the chemical and isotopic analysis of presolar cosmic grains. *Anal. Bioanal. Chem.* **386**, 119-124.
- Berg T., Marosits E., Maul J., Nagel P., Ott U., Schertz F., Schuppler S., Sudek C., and Schönhense G. (2008) Quantum confinement observed in the x-ray absorption spectrum of size distributed meteoritic nanodiamonds. *J. Appl. Phys.*, **104**, 064303.
- Bernatowicz T. J., Gibbons P. C., and Lewis R. S. (1990) Electron energy loss spectrometry of interstellar diamonds. *Astrophys. J.* **359**, 246-255.
- Birrell J., Gerbi J. E., Auciello O., Gibson J. M., Gruen D. M. and Carlisle J. A. (2003) Bonding structure in nitrogen doped ultrananocrystalline diamond. *J. Appl. Phys.* **93**, 5606-5612.
- Blake D., Freund F., Bunch T. (1988) A comparison of Allende diamond with diamond from detonation soot. *Lunar Planet. Sci. Conf.* **XIX**, 94-95 (abstr).



562 Borzdov Yu., Pal'yanov Yu., Kupriyanov I., Gusev V., Khokhryakov A., Sokol A., Efremov  
563 A. (2002) HPHT synthesis of diamond with high nitrogen content from an Fe<sub>3</sub>N–C  
564 system. *Diam. Relat. Mater.* **11**, 1863–1870.

565 Braatz A., Ott U., Henning Th., Jager C. and Jeschke G. (2000) Infrared, ultraviolet, and  
566 electron paramagnetic resonance measurements on presolar diamonds: Implications for  
567 optical features and origin. *Meteoritics & Planet. Sci.* **35**, 75-84.

568 Bradac C., Gaebel T., Naidoo N., Sellars M. J., Twamley J., Brown L. J., Barnard A. S.,  
569 Plakhotnik T., Zvyagin A. V. and Rabeau J. R. (2010) Observation and control of  
570 blinking nitrogen vacancy centres in discrete nanodiamonds. *Nature Nanotechnology* **5**,  
571 345-349.

572 Brydson R., Brown L. M., Bruley J. (1998) Characterising the local nitrogen environment at  
573 platelets in type IaA/B diamond. *J. Microsc.* **189**, 137-144.

574 Buerki P. R., and Leutwyler S. (1991) Homogeneous Nucleation of Diamond Powder by CO<sub>2</sub>  
575 Laser Driven Gas-Phase Reactions. *J. Appl. Phys.*, **69**, 3739–3744.

576 Butenko Yu. V., Coxon P. R., Yeganeh M., Brieva A. C., Liddell K., Dhanak V. R., Šiller L.  
577 (2008) Stability of hydrogenated nanodiamonds under extreme ultraviolet irradiation.  
578 *Diam. Relat. Mater.* **17**, 962–966.

579 Cartigny P., Chinn I., Viljoen K. S., Robinson D. (2004) Early Proterozoic (> 1.8 Ga)  
580 ultrahigh pressure metamorphism: Evidence from Akluilâk microdiamonds (NW  
581 Canada). *Science* **304**, 853-855.

582 Cartigny P. (2005) Stable isotopes and the origin of diamond. *Elements* **1**, 79-84.

583 Clark C. D., Kanda H., Kiflawi I. and Sittas G. (1995) Silicon defect in diamond. *Phys. Rev.*  
584 **B51**, 16681-16688.

585 Daulton T. L., Eisenhour D., Bernatowicz T., Lewis R., and Buseck P. (1996) Genesis of  
586 presolar diamonds: Comparative high-resolution transmission electron microscopy

587 study of meteoritic and terrestrial nanodiamonds. *Geochim. Cosmochim. Acta* **60**, 4853-  
588 4872.

589 Davies G. (1970) No phonon line shapes and crystal strain fields in diamonds. *J. Phys. C:*  
590 *Sol. State Phys.* **3**, 2474-2486.

591 Davies G. (1999) Current problems in diamond: towards a quantitative understanding.  
592 *Physica* **B273-274**, 15-23.

593 Dementjev A. Maslakov K., Kulakova I., Korolkov V., Dolmatov V. (2007) State of C-atoms  
594 on the modified nanodiamond surface. *Diam. Relat. Mater.* **16** 2083–2086.

595 Dolmatov V. Yu. (2007) Detonation-synthesis nanodiamonds: synthesis, structure, properties  
596 and applications. *Russ. Chem. Rev.* **76**, 339-360.

597 Evans T. (1992) Aggregation of nitrogen in diamond. In: *The properties of natural and*  
598 *synthetic diamond* (ed. J. E. Field). Associated Press, London. pp. 259-290.

599 Ferrari A. C. and Robertson J. (2004) Raman spectroscopy of amorphous, nanostructured,  
600 diamond-like carbon, and nanodiamond. *Phil. Trans. R. Soc. Lond. A* **362**, 2477-2512.

601 Fisenko A. V., Verchovsky A. B., Semjonova L. F., and Pillinger C. T. (2001) Heterogeneity  
602 of the interstellar diamond in the CV3 meteorite Efremovka. *Astron. Lett.* **27**, 608-612.

603 Fisenko A. V., Russell S. S., Ash R. D., Semjonova L. F., Verchovsky A. and Pillinger C. T.  
604 (1992) Isotopic composition of carbon and nitrogen in the diamonds from the  
605 unequilibrated ordinary chondrite Krymka LL3.0. *Lunar Planet. Sci. Conf.* **23**, 365-366  
606 (abstr).

607 Fisenko A. V. and Semjonova L. F. (2006) Populations of nanodiamond grains in meteorites  
608 from data on isotopic composition and content of nitrogen. *Solar System Research* **40**,  
609 485-499.

610 Frenklach M., Howard W., Huang D., Yuan J., Sear K. E., Koba R. (1991) Induced  
611 nucleation of diamond powder. *Appl. Phys. Lett.* **59**, 546-549.

612 Hill H. G. M., D'Hendencourt L. B., Perron C., Jones A. P. (1997) Infrared spectroscopy of  
613 interstellar nanodiamonds from the Orgueil meteorite. *Meteoritics Planet. Sci.* **32**, 713-  
614 718.

615 Huss G. R. and Lewis R. S. (1994) Noble gases in presolar diamonds I: Three distinct  
616 components and their implications for diamond origins. *Meteoritics* **29**, 791-810.

617 Iakoubovskii K., Adriaenssens G. J., Vohra Y.K. (2000a) Nitrogen incorporation in diamond  
618 films homoepitaxially grown by chemical vapour deposition. *J. Phys.: Condens. Matter*  
619 **12** L519-L524.

620 Iakoubovskii K., Baidakova M. V., Wouters B. H., Stesmans A., Adriaenssens G. J., Vul' A.  
621 Ya., Grobet P. J. (2000b) Structure and defects of detonation synthesis nanodiamond.  
622 *Diam. Relat. Mater.* **9**, 861-865.

623 Iakoubovskii K., Adriaenssens G. J., Dogadkin N. N., and Shiryayev A. A., (2001) Optical  
624 characterization of 3H, H3 and Si-V centers in diamond. *Diam. Relat. Mater.* **10**, 18-26.

625 Jiang T. and Xu K. (1995) FTIR study of ultradispersed diamond powder synthesised by  
626 explosive detonation. *Carbon* **33**, 1663-1671.

627 Jimenez I., Gago R., Albella J. M., Terminello L. J. (2001) X-ray absorption studies of  
628 bonding environments in graphitic carbon nitride. *Diam. Relat. Mater.* **10**, 1170-1174.

629 Jin S. and Moustakas, T. D. (1994) Effect of nitrogen on the growth of diamond films. *Appl.*  
630 *Phys. Lett.* **65**, 403-405.

631 Knight D. S. and White W. B. (1989) Characterization of diamond films by Raman  
632 spectroscopy. *J. Mater. Res.* **4**, 385-393.

633 Krauss A. R., Gruen D. M., Zhou D., McGauley T. G., Qin L. C., Corrigan T., Auciello O.,  
634 Chang R. P. H. (1998) Morphology and electron emission properties of nanocrystalline  
635 CVD diamond thin films. *Mater. Res. Soc. Symp. Proc.* **495**, 299-310.

636 Kouchi A., Nakano H., Kimura Y., and Kaito C. (2005) Novel route for diamond formation  
637 in interstellar ices and meteoritic parent bodies. *Astrophys. J.* **626**, L129–L132.

638 Kvit A. V., Zhirnov V. V., Tyler T., Hren J. J. (2003) Aging effect and nitrogen distribution  
639 in diamond nanoparticles, *Composites* **B35**, 163–166.

640 Lewis R. S., Anders E., and Draine B. T. (1989) Properties, detectability and origin of  
641 interstellar diamonds in meteorites. *Nature* **339**, 117-121.

642 Lipp M. J., Baonza V. G., Evans W. J., and Lorenzana H. E. (1997) Nanocrystalline  
643 diamond: Effect of confinement, pressure, and heating on phonon modes. *Phys. Rev.*  
644 **B56**, 5978-5984.

645 May P. W. and Mankelevich Yu. A. (2007) The mechanism for Ultrananocrystalline  
646 Diamond Growth: Experimental and Theoretical Studies. *Mater. Res. Soc. Symp. Proc.*  
647 **956**, 0956-J07-04.

648 Morar J. F., Himpsel F. J., Hollinger G., Hughes G., and Jordan J. L. (1985) Observation of C  
649 1s core exciton in diamond. *Phys. Rev. Lett.* **54**, 1960-1963.

650 Mykhaylyk O. O., Solonin Yu. M., Batchelder D. N., Brydson R. (2005) Transformation of  
651 nanodiamond into carbon onions: A comparative study by high-resolution transmission  
652 electron microscopy, electron energy-loss spectroscopy, x-ray diffraction, small-angle  
653 x-ray scattering, and ultraviolet Raman spectroscopy. *J. Appl. Phys.* **97**, 074302-1-15.

654 Newton J., Bischoff A., Arden R. D., Franchi I. A., Geiger T., Greshake A. and Pillinger C.  
655 T. (1995) Acfer 094, a uniquely primitive carbonaceous chondrite from the Sahara.  
656 *Meteoritics* **30**, 47-56.

657 Nuth J. A. and Allenn J. E. Jr. (1992) Supernovae as sources of interstellar diamonds.  
658 *Astrophysics Space Sci.* **196**, 117-123.

659 Orlinskii S. B., Bogomolov R. S., Kiyamova A. M., Yavkin B. V., Mamin G. M., Turner S.,  
660 van Tendeloo G., Shiryaev A. A., Vlasov I. I. and Shenderova O. (2011) Identification  
661 of Substitutional Nitrogen and Surface Paramagnetic Centers in Nanodiamond of  
662 Dynamic Synthesis by Electron Paramagnetic Resonance. *Nanosci. & Nanotech. Lett.*  
663 **3**, 63–67.

664 Pichot V., Stephan O., Comet M., Fousson E., Mory J., March K., and Spitzer D. (2010) High  
665 Nitrogen Doping of Detonation Nanodiamonds. *J. Phys. Chem. C.* **114**, 10082–10087.

666 Russell S. S., Arden J. W., and Pillinger C. T. (1996) A carbon and nitrogen isotopic study of  
667 diamond from primitive chondrites. *Meteoritics and Planet. Sci.* **31**, 343-355.

668 Samlenski R., Haug C., Brenn R., Wild C., Locher R., and Koidl P. (1995) Incorporation of  
669 nitrogen in chemical vapor deposition diamond. *Appl. Phys. Lett.* **67**, 2798-2800.

670 Saslaw W. C. and Gaustad J. E. (1969) Interstellar dust and diamond. *Nature* **221**, 160-162.

671 Sellschop J. P. F. (1992) Nuclear probes in the study of diamond. In: *The properties of*  
672 *natural and synthetic diamond* (ed. J. E. Field), Associated Press, London. pp. 81-180.

673 Shiryaev A. A., Fisenko A. V., Krivobok V. S., Vlasov I. I., Semjonova L. F. (2009) Nitrogen  
674 in Meteoritic Nanodiamonds: Lattice Impurity in Diamond Core or a Constituent of an  
675 Associated Carbonaceous Phases? *Lunar Planet. Sci. Conf.* **40**, 1317 (abstr).

676 Smith B. R., Inglis D. W., Sandnes B., Rabeau J. R., Zvyagin A. V., Gruber D., Noble C. J.,  
677 Vogel R., Osawa E., Plakhotnik T. (2008) Five-nanometer diamond with luminescent  
678 nitrogen-vacancy defect centers. *Small* **5**, 1649-1653.

679 Staver A. M., Ershov A. P. and Lyamkin A. I. (1984) Study of detonations in condensed  
680 explosives by conduction methods. *Combustion, Explosion, and Shock Waves*, **20**, 320-  
681 324.

682 Tang M., Lewis R. S., Anders E., Grady M. M., Wright I. P., and Pillinger C. T. (1988)  
683 Isotopic anomalies of Ne, Xe and C in meteorites. I. Separation of carriers by density  
684 and chemical resistance. *Geochim. Cosmochim. Acta* **52**, 1221-1234.

685 Titantah J. T. and Lamoen D. (2007) Carbon and nitrogen 1s energy levels in amorphous  
686 carbon nitride systems: XPS interpretation using first-principles. *Diam. Relat. Mater.*  
687 **16**, 581–588.

688 Turner S., Lebedev O. I., Shenderova O., Vlasov I. I., Verbeeck J., and van Tendeloo G.  
689 (2009) Determination of Size, Morphology, and Nitrogen Impurity Location in Treated  
690 Detonation Nanodiamond by Transmission Electron Microscopy. *Adv. Funct. Mater.*  
691 **19**, 2116–2124.

692 Vavilov V. S., Gippius A. A., Zaitsev A. M., Deryagin, B. V., Spitsyn B. V. and Aleksenko  
693 A. E. (1980) Investigation of the cathodoluminescence of epitaxial diamond films. *Sov.*  
694 *Phys. Semicond.* **14**, 1078-1079.

695 Verchovsky A. B., Fisenko A. V., Semjonova L. F., Wright I. P., Lee M. R., and Pillinger C.  
696 T. (1998) Noble gas isotopes in grain size separates of presolar diamonds from  
697 Efremovka. *Science* **281**, 1165-1168.

698 Vlasov I. I., Barnard A. S., Ralchenko V. G., Lebedev O. I., Kanzyuba M.V., Konov V. I.,  
699 and Goovaerts E., (2009) Nanodiamond photoemitters based on strong narrow-band  
700 luminescence from silicon-vacancy defects, *Adv. Mater.*, **21**, 808-812.

701 Vlasov I. I., Shenderova O., Turner S., Lebedev O. I., Basov A. A., Sildos I., Rähn M.,  
702 Shiryayev A. A., and van Tendeloo G. (2010) Nitrogen and Luminescent Nitrogen-  
703 Vacancy Defects in Detonation Nanodiamond. *Small*, **6**, 687-694.

704 Vul' A. Ya. (2006) Characterisation and physical properties of UNCD particles. In  
705 *Ultrananocrystalline Diamond* (Eds: O. Shenderova, D. Gruen), William-Andrew,  
706 Norwich, NY. 379-404.

- 707 Zaitsev, A.M. (2001) *Optical Properties of Diamond*. Springer, Berlin.
- 708 Zaitsev A. M., Vavilov V. S. and Gippius A. A. (1981) *Sov. Phys .Lebedev Inst. Rep.* **10**, 15-  
709 20.
- 710 Zapol P., Sternberg M., Curtiss L. A., Frauenheim T., Gruen D. M. (2001) Tight-binding  
711 molecular-dynamics simulation of impurities in ultrananocrystalline diamond grain  
712 boundaries *Phys. Rev.* **B65**, 045403.
- 713 Zhang G. F., Geng D. S., Yang Z. J. (1999) High nitrogen amounts incorporated diamond  
714 films deposited by the addition of nitrogen in a hot-filament CVD system. *Surface*  
715 *Coatings Technology* **122**, 268–272.
- 716 Zhdankina O. Yu., Zadneprovskii B. I., Artemenko V. V., Kulakova I. I., Rudenko A. P.  
717 (1986) Influence of concentration of paramagnetic nitrogen on oxidation kinetics of  
718 synthetic diamonds of various morphologies. *Bull. Moscow State Univ. Chem.* **27**, 293-  
719 297.

## Figure captions

720

721

722 **Figure 1.** X-ray diffraction pattern of nanodiamond from Efremovka chondrite.  
723 Monochromatic molybdenum radiation was employed. Numbers show Miller indexes of the  
724 diamond reflections.

725

726 **Figure 2.** Raman spectra of meteoritic nanodiamond from Efremovka meteorites  
727 recorded using ultra-violet (244 nm) excitation. The Orgueil MND are marked as OD; the  
728 Efremovka MND are marked as DE; the synthetic detonation nanodiamond as UDD.

729

730 **Figure 3.** Photoluminescence spectra of meteoritic nanodiamonds recorded at 488 nm  
731 excitation at room temperature. Typical spectrum of the nanodiamond made by detonation is  
732 also shown. The arrow points to the main and secondary lines of the Si-V defect. All spectra  
733 are normalized and are displaced vertically for clarity. The figure B shows enlarged spectral  
734 region where the Si-V defect is observed. The curves are *not* displaced vertically, but are  
735 normalized to the maximum of the band at 550-600 nm. For comparison a spectrum of a Si-V  
736 defect in nanocrystalline CVD film is shown (Vlasov et al., 2009).

737

738 **Figure 4.** Photoemission (PEEM) image of a Si plate with precipitated nanodiamond  
739 from Orgueil meteorite (bright white bands) at the C absorption edge. The field of view is 37  
740 microns.

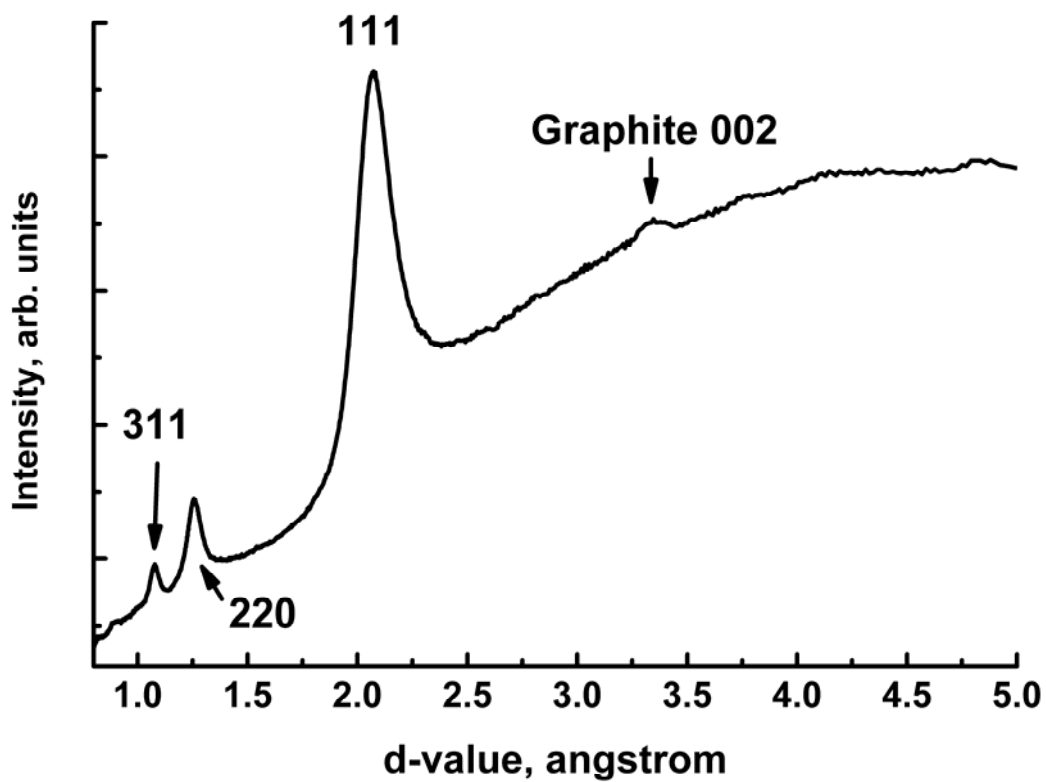
741

742 **Figure 5.** NEXAFS spectra at carbon (A) and nitrogen (B) absorption edges of the  
743 meteoritic nanodiamond from Orgueil (MND) and detonation (UDD) nanodiamond. Figure C  
744 shows calculated NEXAFS spectra of various configurations of nitrogen in cubic (c-dia) and



745 hexagonal (h-dia) diamond lattices. The curves are displaced vertically for clarity; horizontal  
746 axis shows energy relative to the absorption edge. Marked differences between the shapes of  
747 the experimental and modeled absorption spectra are obvious.

748



749

750

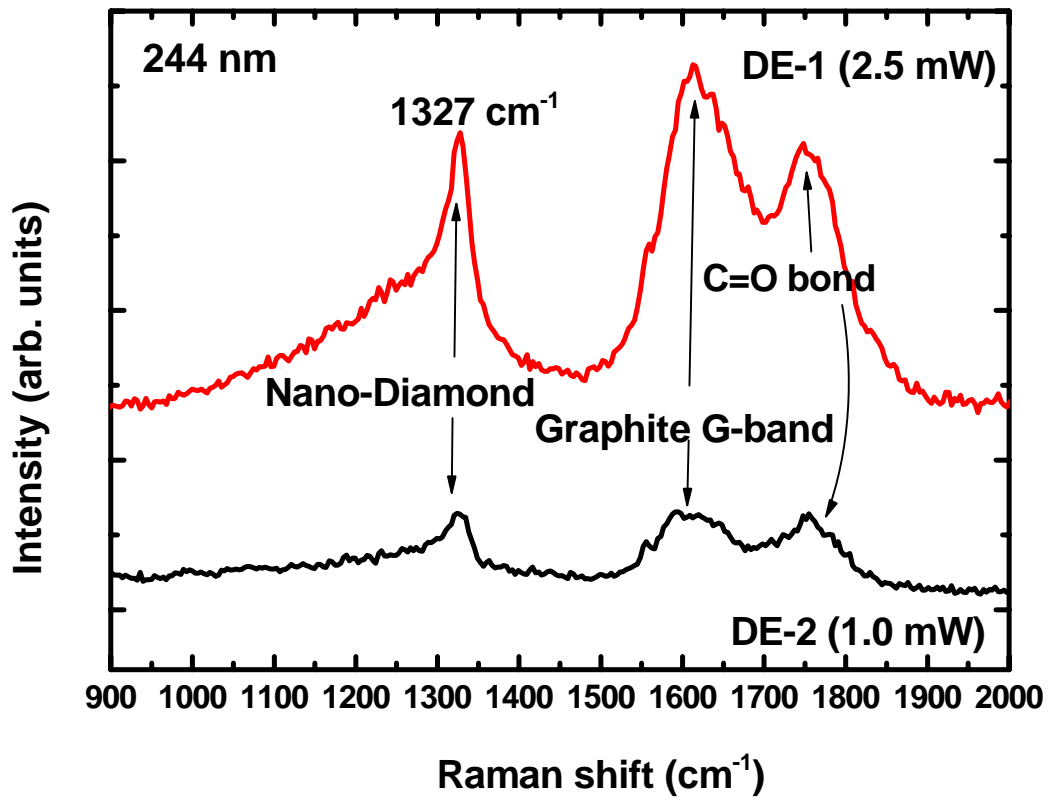
751

752

753

754

Figure 1.



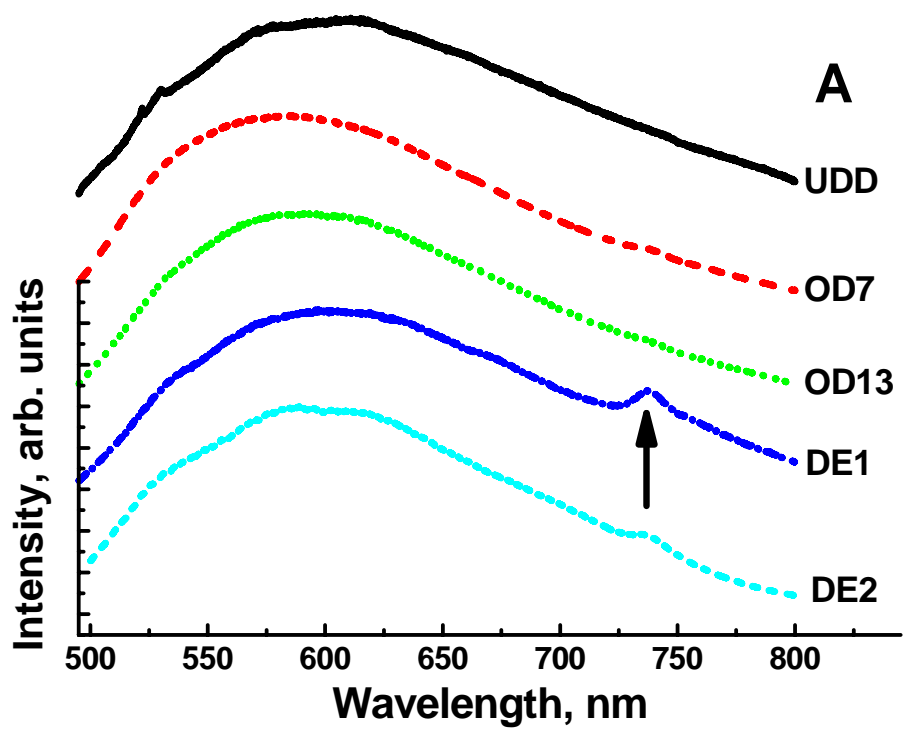
755  
756

757

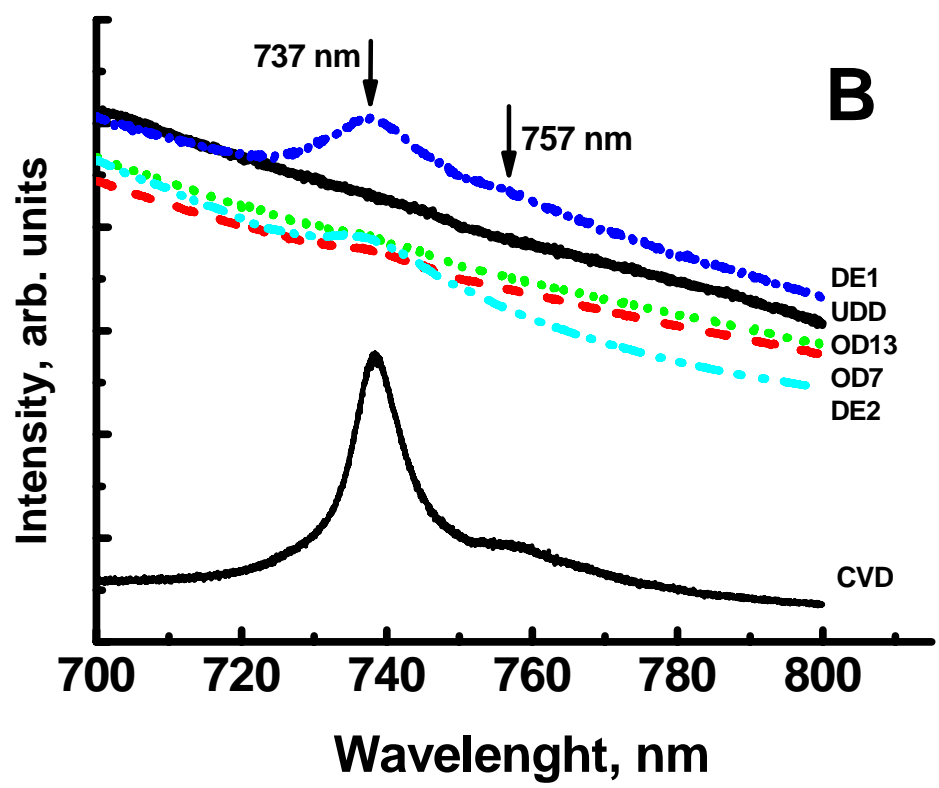
758

Figure 2.

759



760



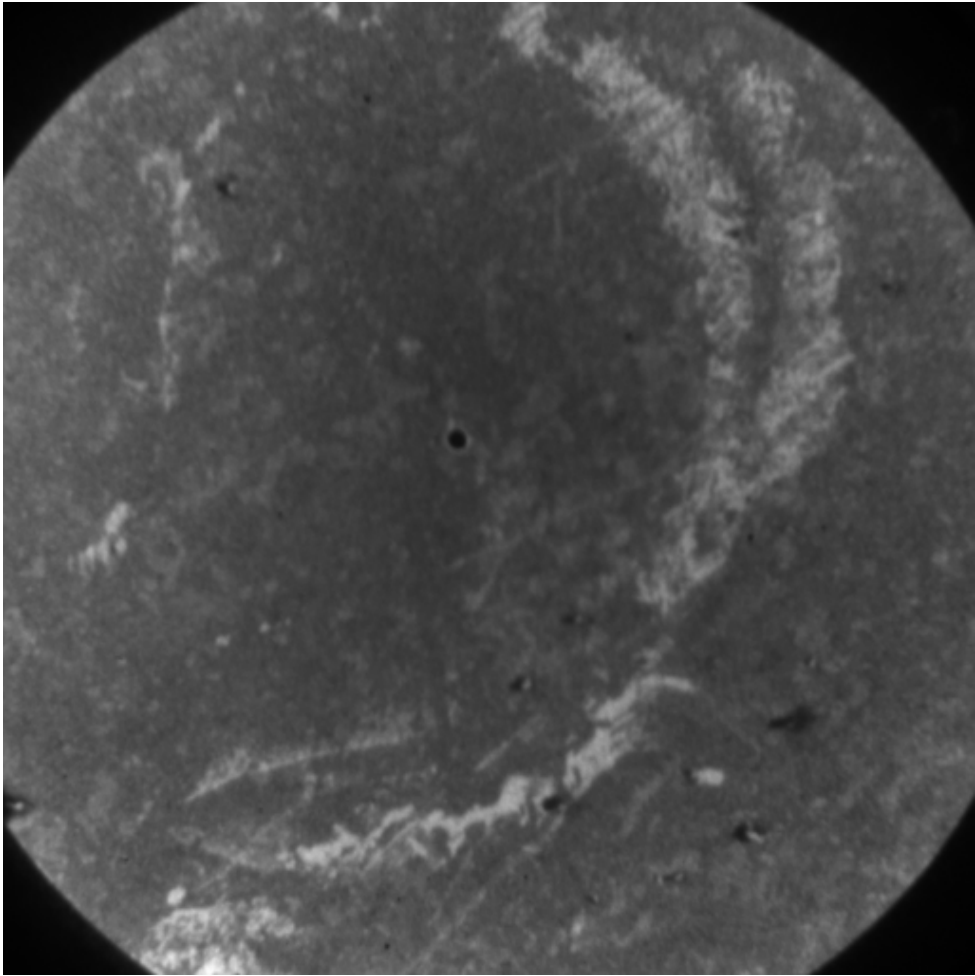
761

762

763

Figure 3.

764



765

766

767

**Figure 4.**

768

769

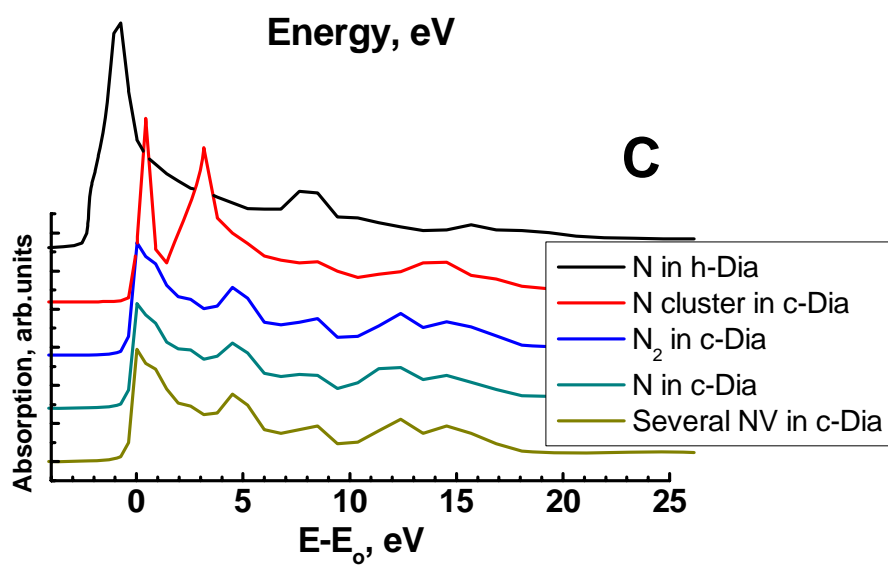
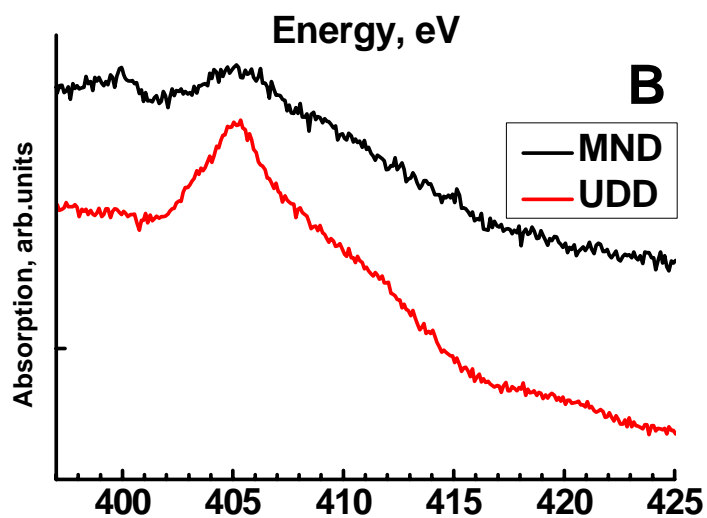
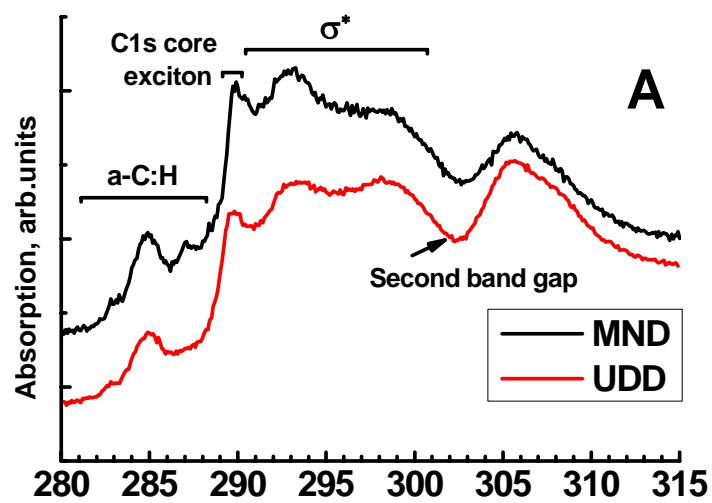


Figure 5.